

Effects of Magnetic Field Distribution on Power Absorption through Second Harmonic Electron Cyclotron Resonance Heating in Mirror Machines

TATEMATSU Yoshinori, SAITO Teruo, KATANUMA Isao and CHO Teruji

Plasma Research Center, University of Tsukuba

Ibaraki 305-8577, Japan

(Received: 9 December 2003 / Accepted: 17 April 2004)

Abstract

Absorption of microwave power at second harmonic electron cyclotron resonance is investigated by ray tracing calculations for three positions in the GAMMA 10 tandem mirror with different magnetic field configurations. The magnitude of absorption depends on the magnetic field distribution along the ray of the wave. The optical depth is proportional to square root of the on-axis electron temperature T_e for rays along which the magnetic field strength is almost constant while the optical depth is proportional to T_e for the rays that see a large magnetic field gradient. The magnetic field with a large magnetic scale length is favorable for strong power absorption but sensitive for a magnetic field change and it is difficult to control a spatial absorption profile

Keywords:

ray tracing, ECRH, second harmonic, optical depth, magnetic field distribution

1. Introduction

Microwaves of 28 GHz are injected in the plug/barrier and the central cells for creating a plasma confining potential and raising the electron temperature in the GAMMA 10 tandem mirror [1,2]. Here, fundamental and second harmonic electron cyclotron resonance heating (ECRH) have been employed. Power absorption due to ECRH depends on the magnetic field distribution along the path of the microwave. In order to find the best magnetic field configuration, ray tracing has been used [3], and the dependence of microwave absorption on plasma parameters was theoretically investigated in a non-uniform magnetic field for fundamental heating [4-6] and for second harmonic heating [7]. Since it is experimentally found that the spatial profile of power absorption strongly affects the property of plasma confinement [8,9], it is important to investigate the ways to control the absorption profile. Moreover, as a result of second harmonic ECRH, reduction of electron drag was attained in the central cell [10].

In the present paper, absorption rate and its spatial distribution of the heating microwave power are investigated for second harmonic ECRH. The power absorption is evaluated with ray tracing calculations for three different magnetic field distributions in the central cell, the barrier and the plug regions in GAMMA 10 and we study the effects of the magnetic field configuration on power absorption. Absorption coefficients depend on the plasma density, the electron tem-

perature and the magnetic field distributions along the rays. Plasma density in the central cell is about ten times larger than that in the plug/barrier cell, and the scale length of the magnetic field in the central resonance region is much longer than that in the plug region. Thus, the absorption rate is expected to be much larger in the central cell than in the plug/barrier cell for the second harmonic ECRH.

The outline of the present paper is as follows; the ECRH systems and magnetic field configuration of GAMMA 10 are described in Sec. 2. Calculations of ray tracing are presented in Sec. 3. Then, discussion and summary are described.

2. ECRH systems and magnetic field configuration

Microwaves of 28 GHz are generated by gyrotrons with a circular TE_{02} mode for the ECRH in GAMMA 10. They are transmitted through waveguides and are radiated to the plasma as linearly polarized waves from Vlasov antennas. Several Vlasov antennas have been installed in the central and the plug/barrier cells in GAMMA 10. Table 1 shows the characteristics of them. Plug-antennas, P, have been settled for creation of the ion confining potential and barrier antennas, B, contribute to hot electron generation and formation of the thermal barrier potential. A central-cell antenna, C, has been used to raise the electron temperature in the main plasma confining region. The central- and the barrier-ECRH sys-

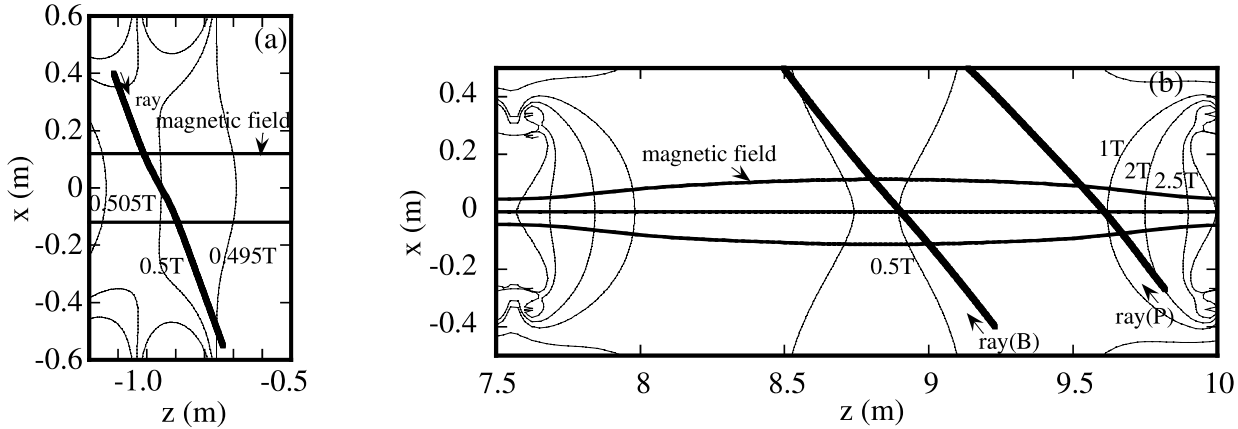


Fig. 1 Calculated rays are shown (the thickest lines) for (a) the central region and (b) the plug/barrier region. The thin curves represent the contours of magnetic field strength and the middle thick curves show magnetic lines of force.

Table 1 Characteristics of the ECRH antennas in GAMMA 10. The symbols θ_z and θ_B represent the incident angles of the microwave from the GAMMA 10 axis and the magnetic field line at launching points, respectively, q_x is the ratio of the X-mode included in the microwave and L_B is the magnetic scale length along the axis at the resonance point.

name	harmonic	θ_z	θ_B	q_x	L_B (m)
C	$2\omega_c$	67°	67°	0.74	~ 25
B	$2\omega_c$	50°	57°	0.68	~ 5
P	ω_c	50°	87°	0.99	~ 0.4

tems are used for the 2nd harmonic heating and the plug one has been used for the fundamental heating.

The magnetic field distributions of the central and plug/barrier cells are shown in Figs. 1(a) and 1(b), respectively. Thin curves show the contours of the magnetic field strength and middle thick curves show the magnetic lines of force. The resonance magnetic field strengths are 1 T and 0.5 T for the fundamental and the second harmonic resonance heating, respectively.

In typical experiments in GAMMA 10, square of the ratio of the plasma frequency to the wave frequency $(\omega_p/\omega)^2$ is about 0.2 and 0.02 on axis in the central and plug/barrier cells, respectively. The electron temperature is several tens of eV and several hundreds of eV, respectively, under the plug- and barrier-ECRH operations.

3. Ray-tracing

We investigate the effect of magnetic field distributions on ECRH and we calculate the power absorption for 2nd harmonic heating. As for the plug-ECRH, 56GHz microwave is virtually injected with the same incident angle as the actual ray of 28 GHz and its absorption power through the 2nd harmonic resonance in the plug magnetic field is calculated with the ray-tracing code. Since the microwave power is well absorbed for X-mode injection at the second harmonic resonance, we trace the rays of the X-mode.

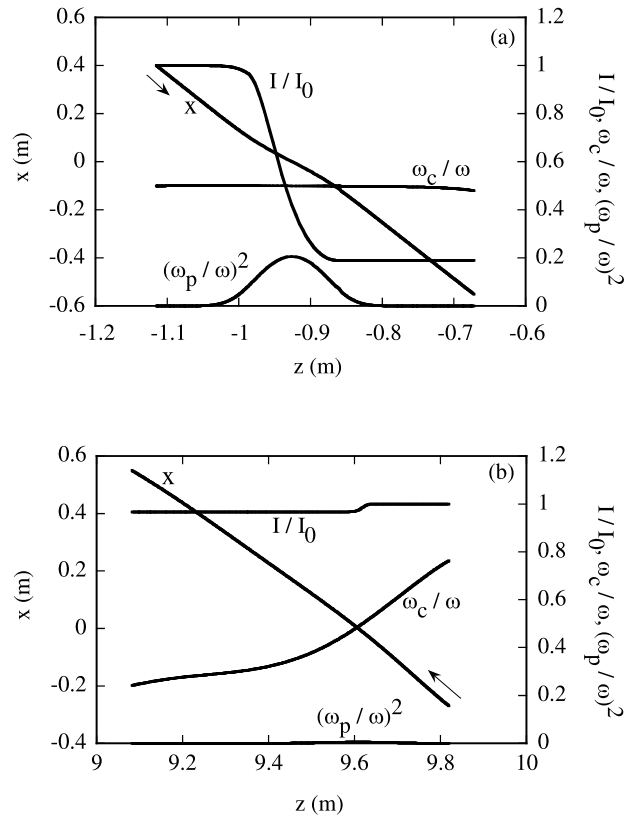


Fig. 2 Position x , normalized density $(\omega_p/\omega)^2$, magnetic field strength ω_c/ω , and intensity normalized by the initial I/I_0 are plotted against axial coordinate z along the rays for (a) central-ECRH and (b) plug-ECRH.

The calculated rays are shown in Fig. 1 with the thick lines. Figure 1(a) shows the center ray radiated from the C antenna and Fig. 1(b) shows those radiated from the B and the P antennas. The magnetic field strength of 0.5 T corresponds to the resonance point for the central- and the barrier-ECRH and 1 T is the resonance one for the plug-ECRH with the 56 GHz microwave.

Spatial profiles of the electron density and temperature adopted in the calculations are $n_e(\psi) = n_{e0} \exp(-\psi/\psi_n)$ and

$T_e(\psi) = T_{e0} \exp(-\psi/\psi_T)$, respectively, where ψ is the magnetic flux. In the following calculations, $n_{e0} = 2 \times 10^{12} \text{ cm}^{-3}$ and $T_{e0} = 0.1 \text{ keV}$ for the central-rays and $n_{e0} = 2 \times 10^{11} \text{ cm}^{-3}$ and $T_{e0} = 1 \text{ keV}$ for the barrier- and the plug-rays are assumed.

Figure 2 (a) plots variations of the x -coordinate, the normalized density, $(\omega_p/\omega)^2$, the normalized magnetic field strength, ω_c/ω , and the normalized intensity, I/I_0 , along the ray emitted from the C antenna against the axial coordinate, z . Here, ω_p and ω_c indicate the local electron plasma and cyclotron frequencies, respectively. A large fraction of the microwave power is absorbed as the density increases and about 80% of the incident power is absorbed.

The same calculations for the plug-ECRH are shown in Fig. 2(b). The launching point of the microwave is $z = 9.82 \text{ m}$ and the ray proceeds from the right to the left in Fig. 2(b). The electron density at the plug is so low, one-tenth times as large as that at the central cell, that the absorption rate of the incident power is only about several percent. Microwave power is absorbed in the narrow region where the resonance condition is satisfied.

The variations of the magnetic field strength along the rays for the central-, the plug- and the barrier-ECRH are plotted in Fig. 3. The density profile used in calculation for central-ECRH is also indicated in Fig. 3. The remarkable difference of the results between the central and the plug ray-tracings is the amount of variation of the magnetic field strength along the rays. For the central- and the barrier-ECRH, the resonance regions locate near the mid-plane and the magnetic field strength is almost constant along the ray. On the other hand, the magnetic field strength substantially varies for the plug ray owing to a large magnetic field gradient.

Next, variation of the absorption rate with the magnetic field strength along the rays is investigated. Normalized absorption rates are plotted for X-mode microwaves emitted from the three antennas in Fig. 4. The magnetic field strengths are uniformly changed. The absorption for the central-ECRH drastically decreases for a slight variation from

the standard value used in the GAMMA 10 experiments. On the other hand, absorption for the plug-ECRH does not vary very much.

The temperature dependence of the absorption rate is also investigated. Figure 5 plots the absorption rates as a function of the on-axis electron temperature T_{e0} . Assumed densities on axis are $2 \times 10^{11} \text{ cm}^{-3}$, $1 \times 10^{11} \text{ cm}^{-3}$ and $4 \times 10^{11} \text{ cm}^{-3}$ for the central, barrier and plug plasma, respectively, in the calculations, which are different from their actual values, to make sure of the temperature dependence of the absorption rate. The absorption rates are fitted to curves of $1 - \exp(-q)$ and $q \propto T_{e0}^m$, with m being a fitting parameter. The value of m is nearly equal to 0.5 for the central and the barrier rays, and 1 for the plug ray.

4. Discussion

The parameter q in the previous section corresponds to the optical depth and it is calculated as $q = \int 2k_i ds$ where k_i is the imaginary part of the complex wave number and s is the coordinate along the ray. The expression of k_i for 2nd harmonic ECRH is [11],

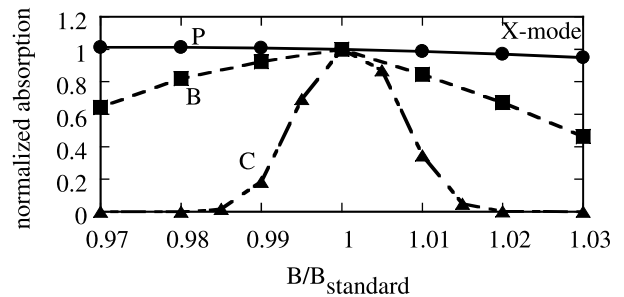


Fig. 4 Normalized absorption rates against the variation of background magnetic field strength for the central, the barrier and the plug rays. The magnetic field strength is normalized by the standard value used in the GAMMA experiments.

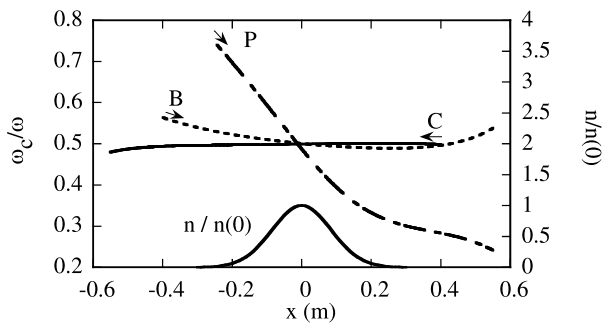


Fig. 3 The normalized magnetic field strength ω_c/ω is plotted along the rays emitted from C (the solid curve), P (the dashed curve) and B (the dotted curve) antennas. The normalized density distribution in the central cell is also plotted.

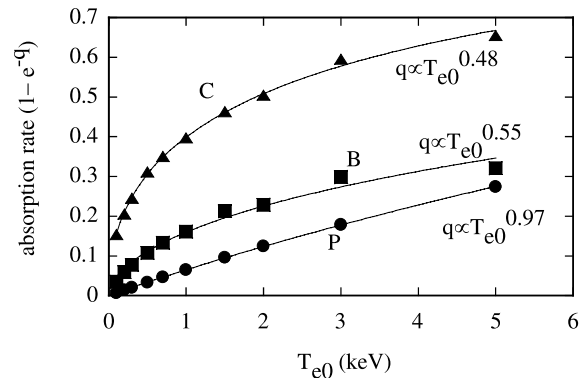


Fig. 5 Absorption rates against on-axis-temperature for C, B and P antennas. The plots are fitted with $1 - e^{-q}$.

$$k_i = \sqrt{\pi} \frac{\omega_p^2}{\omega^2} \frac{kk_{\perp}^2}{m\omega_c^2} \frac{\omega T_e}{k_{\parallel}v} \exp\left[-\left(\frac{\omega - 2\omega_c}{k_{\parallel}v}\right)^2\right], \quad (1)$$

where k , k_{\parallel} and k_{\perp} are the real part of the wave number, its parallel and perpendicular components to magnetic field, respectively, m is electron mass and $mv^2/2 = T_e$. We transform the coordinate s to $\eta = (\omega - 2\omega_c)/\omega$, then

$$q \propto \int \frac{T_e}{k_{\parallel}v} \exp\left(-\frac{\omega^2}{k_{\parallel}^2 v^2} \eta^2\right) d\eta. \quad (2)$$

We evaluate η for the rays in the central cell and the barrier regions. Since the magnetic field strength along the rays is almost constant satisfying $\eta \approx 0$ for these rays, we can substitute $\eta = 0$ in place of integral in eq. (2), and $q \propto T_e^{1/2}$ is obtained. On the other hand, for the rays along which the magnetic field strength widely varies, the upper and lower limits of the integral can be replaced by $\pm\infty$ and $q \propto T_e$ is obtained. These results agree with the ray-tracing calculations. Thus, the magnetic field distribution along the rays affects the absorption rate for 2nd harmonic ECRH.

Difference of the magnetic scale length strongly affects the heating efficiency and the heating pattern can be controlled. Since absorption region is narrow along the magnetic axis for the plug-ECRH, local heating is realized. On the other hand, the scale length is so long that the beam width determines the heating region along the axis for the central-ECRH. The magnetic field distribution with a large scale length is favorable for heating efficiency, but it is difficult to control the spatial distribution of power absorption. It is found that the absorption rate is very sensitive to the variation of the central cell magnetic field, because a large shift of the resonance point occurs against a slight variation of the magnetic field strength and resonance point disappears from

the region of the heating microwave beam.

5. Summary

Ray tracing calculations are carried out and the absorption rates of microwave power for 2nd harmonic ECRH are evaluated in the central, the barrier and the plug regions in the GAMMA 10 tandem mirror. The power absorption in the central cell in which the rays see almost constant magnetic field strength is largely affected by a small background magnetic field deviation. The temperature dependence of the absorption rates is well explained by the magnetic field distributions along the rays. Optical depth of the injected microwave is proportional to square root of the on-axis electron temperature T_e for rays with almost constant magnetic field strength and is proportional to T_e for the rays with a large magnetic field gradient.

The authors wish to thank the members of the GAMMA 10 group for stimulating discussions.

References

- [1] Y. Kiwamoto *et al.*, *Phys. Fluids* **29**, 2781 (1986).
- [2] T. Cho *et al.*, *Nucl. Fusion* **27**, 1421 (1987).
- [3] T. Saito *et al.*, *Nucl. Fusion* **30**, 1533 (1990).
- [4] Y. Kiwamoto *et al.*, *Phys. Plasmas* **1**, 834 (1994).
- [5] Y. Kiwamoto *et al.*, *Phys. Plasmas* **1**, 3986 (1994).
- [6] Y. Tatematsu *et al.*, *Phys. Plasmas* **3**, 3318 (1996).
- [7] Y. Tatematsu *et al.*, *Phys. Plasmas* **4**, 2972 (1997).
- [8] K. Yatsu *et al.*, *J. Plasma Fusion Res.* **74**, 844 (1999).
- [9] T. Saito *et al.*, *Fusion Eng. Des.* **53**, 267 (2001).
- [10] T. Saito *et al.*, *Fusion Energy* 1996, **2**, 105 (IAEA, VIENNA, 1997).
- [11] T. H. Stix, in *Waves in Plasmas* (AIP, 1992).